

Influence of silicon ion implantation on the morphological features, structural properties, optical, and electrical behavior of CR-39 polymers

Bashir S, Ahmad S, Ali N, Umm-i-Kalsoom, Rafique M S, and Husinsky W

Citation: Chin. Phys. B, 2026, 35 (**7**): 070707. DOI: 10.1088/1674-1056/ae39db
http://cpb.iphy.ac.cn; http://iopscience.iop.org/cpb

What follows is a list of articles you may be interested in

Fast compressed sensing spectral measurement with adaptive gradient multiscale resolution

Ruo-Ming Lan(蓝若明), Xue-Feng Liu(刘雪峰), Tian-Ping Li(李天平), and Cheng-Jie Bai(白成杰)
Chin. Phys. B, 2024, 33 (**2**): 020702. DOI: 10.1088/1674-1056/ad09cf

Synchronous detection of multiple optical characteristics of atmospheric aerosol by coupled photoacoustic cavity

Hua-Wei Jin(靳华伟), Ren-Zhi Hu(胡仁志), Pin-Hua Xie(谢品华), and Ping Luo(罗平)
Chin. Phys. B, 2022, 31 (**6**): 060703. DOI: 10.1088/1674-1056/ac43ad

Phase transition of shocked water up to 6 GPa: Transmittance investigation

Lang Wu(吴浪), Yue-Hong Ren(任月虹), Wen-Qiang Liao(廖文强), Xi-Chen Huang(黄曦晨), Fu-Sheng Liu(刘福生), Ming-Jian Zhang(张明建), and Yan-Yun Sun(孙燕云)
Chin. Phys. B, 2021, 30 (**5**): 050701. DOI: 10.1088/1674-1056/abd691

Super-resolution imaging of low-contrast periodic nanoparticle arrays by microsphere-assisted microscopy

Qin-Fang Shi(石勤芳), Song-Lin Yang(杨松林), Yu-Rong Cao(曹玉蓉), Xiao-Qing Wang(王晓晴), Tao Chen(陈涛), and Yong-Hong Ye(叶永红)
Chin. Phys. B, 2021, 30 (**4**): 040702. DOI: 10.1088/1674-1056/abcf48

Design of NO_2 photoacoustic sensor with high reflective mirror based on low power blue diode laser

Hua-Wei Jin(靳华伟), Pin-Hua Xie(谢品华), Ren-Zhi Hu(胡仁志), Chong-Chong Huang(黄崇崇), Chuan Lin(林川), Feng-Yang Wang(王凤阳)
Chin. Phys. B, 2020, 29 (**6**): 060701. DOI: 10.1088/1674-1056/ab8376

Influence of silicon ion implantation on the morphological features, structural properties, optical, and electrical behavior of CR-39 polymers

Bashir S[1,2], Ahmad S[3], Ali N[4,6], Umm-i-Kalsoom[4,6,†], Rafique M S[5], and Husinsky W[6]

[1] *Department of Physics, Government College University, Lahore* 54000, *Pakistan*
[2] *Government College Women University, Sialkot* 52, *Pakistan*
[3] *Centre for Advanced Studies in Physics, Government College University, Lahore* 54000, *Pakistan*
[4] *Department of Natural Sciences and Humanities, University of Engineering and Technology Lahore, New Campus, Kalashah Kaku, Sheikhupura* 39020, *Pakistan*
[5] *Department of Physics, University of Engineering and Technology, Lahore* 54000, *Pakistan*
[6] *Institute for Applied Physics, Vienna University of Technology, Wiedner Hauptstr.* 8–10/134, *A-1040 Wien, Austria*

(Received 30 April 2025; revised manuscript received 5 January 2026; accepted manuscript online 19 January 2026)

The variations in morphological features, structural properties, optical characteristics, and electrical behavior induced by 610-keV Si ions in the CR-39 matrix have been investigated in the current research work. Polymer targets were irradiated with Si ions for various fluences spanning from 5×10^{13} ions/cm^2 to 35×10^{16} ions/cm^2. The implantation of ions in the polymeric target generally leads to chain scission, bond breaking, and cross-linking, along with the formation of free radicals and ions. To confirm these effects, various characterization techniques have been utilized. Optical microscopy reveals the creation of micro-cavities and cracks along the grain boundaries. Confocal microscopy demonstrates the formation of micro-sized hillocks. The formation of SiC phase at 890 cm^{-1} following ion implantation was identified by Raman spectroscopy. Furthermore, in CR-39, a significant reduction in optical transmittance in the visible region is attributable to the formation of Si and carbonaceous clusters on the target surface. The enhancement in the electrical conductivity of the Si ion implanted polymer with an increase in ion fluence is attributable to fine crystallinity and the development of SiC bridges. The assessed temperature of the surface of the implanted polymer ranges from 2.2×10^4 K to 6.2×10^4 K. The LET (total linear energy transfer) value of 610-keV implanted ions and their depth are 63 eV/Å and 1.11 μm recorded in CR-39, respectively, estimated by SRIM simulation. The improved morphological features, structural properties, optical characteristics, and electrical behavior of CR-39 make it beneficial for applications in packaging and electronic industries, medical sciences, and photonic devices.

Keywords: surface morphology, carbonaceous clusters, optical transmittance, structural modification

PACS: 07.60.Pb, 07.79.Lh, 07.60.Rd, 06.60.Ei

DOI: 10.1088/1674-1056/ae39db **CSTR:** 32038.14.CPB.ae39db

1. Introduction

Ion implantation technique makes extensive use of a wide range of ion sources, such as linear accelerator ion sources (LAIS), electron beam ion sources (EBIS), electron cyclotron resonance (ECR) sources, and metal vapor vacuum arc ion sources (MVVAIS). Although these traditional sources can produce Si ions with regulated charge states and energies, they often require longer implantation times and give comparatively low instantaneous ion fluence. Using laser-generated plasma as an ion source, which provides high ion fluence, short ion pulse duration, numerous charge states, and adjustable energy distributions under extremely non-equilibrium conditions, can get around this restriction. An external magnetic field can be used to further improve the energy, ion charge state, fluence, yield, and plasma lifespan. Wake field effects, plasma confinement, emission enhancement, and plasma instabilities all contribute significantly to the improvement of ion energy, fluence, yield, signal sensitivity, repeatability, and plasma lifespan during plasma expansion in the presence of a magnetic field. The Si ions can also be produced by conventional ion accelerators at similar nominal energies, while laser-driven plasma ion sources provide distinct advantages in terms of short irradiation times, high instantaneous ion flux, and non-equilibrium ion–matter interactions. These characteristics justify the novelty, uniqueness, and efficacy of the technology used in this work by making laser-generated plasma especially appropriate for causing structural alterations in polymeric materials.[1–7] Torrisi *et al.*[3] reported that the average ionic energy of the order of 122%, 18%, and 161% of charge state 1^+ for the Cu, Al, and Ta ions is increased due to the existence of an externally applied magnetic field. The states of charge and kinetic energy of plasma ions depend upon parameters of the laser, laser pulse energy, pulse number, laser pulse duration, chemical compositions of the irradiated target

[†]Corresponding author. E-mail: ummikalsoom@uet.edu.pk

© 2026 Chinese Physical Society and IOP Publishing Ltd. All rights, including for text and data mining, AI training, and similar technologies, are reserved.

material, the strength of the magnetic field, and the irradiation angle.[7]

Poly-allyl-diglycol-carbonate (CR-39) have vast range of applications in field of technology, science, medical, optics, biotechnology, opto-electronics, photonics, electrical devices, and space science.[8,9] Due to their distinctive properties specifically, low density, versatile electronic properties, ability to form intricate shape/size and low cost of manufacturing with highest sensitivity.[10,11] The surface, optical, structural, and electrical properties of various insulating polymers are enhanced using diverse scientific techniques under appropriate conditions.[12,13] Ion implantation produced by the laser is versatile and effective technique that can be performed in a controlled manner.[5] Elevated momentum and energy deposition in a trivial cylindrical zone of polymer target surface and subsurface around the latent track, *i.e.*, the path of implanted ion, is the famous feature of ion implantation.[14] The latent tracks formation in the surface and subsurface of polymer target is due to growth of unsaturated bonds, triple bonds, and volatile fragments losses. After ion implantation dramatic modifications take place in the properties of polymer and are attributed to the breaking of covalent bonds, scissoring of long polymeric chains, carbon clusters formation, new chemical bonds formations, and volatile species liberation. These processes can cause variation in the surface, structural electrical, optical, and mechanical characteristics of polymer CR-39.[15–18]

Current work focuses on the enhancement in optical and electrical characteristics of polymer targets in the intermediate ion fluence range from 5×10^{13} ions $\cdot$ cm^{-2} to 35×10^{16} ions $\cdot$ cm^{-2}. The choice of high ion fluences up to 35×10^{16} ions/cm^2 was intentional to induce substantial structural and chemical modifications in CR-39, enabling us to explore its phase transformation behavior under extreme irradiation conditions. While CR-39 is not traditionally classified as a radiation-hard material, several studies have shown that polymers can undergo significant property changes such as cross-linking, carbonization, clustering of sp^2–carbon bonds, phase reorganization, and enhanced conductivity for fluence values comparable to 10^{16} ions/cm^2.[19–21] Some theoretical models collectively explain how high-fluence ion irradiation drives beneficial transformations in materials like CR-39. This occurs through localized energy deposition, atomic displacements, and thermal effects. Laser-induced ion irradiation effects can be briefly discussed based on different models. These theoretical models collectively explain how high-fluence ion irradiation drives beneficial transformations in materials like CR-39. This phenomenon occurs via localized energy deposition, atomic displacements, and thermal effects. They support phenomena such as SiC formation, conductivity improvement, and microstructural reorganization, validating the observed experimental outcomes. Using the thermal-spike model, one can describe the abrupt and localized energy absorption/deposition along the ion tracks. This produces transient local elevations in pressure and temperature, enabling rehybridization, local phase transformations (*e.g.*, carbon clusters & SiC formations detectable by Raman spectroscopy), bond breaking, and enhanced conductivity.[20,22] Defect complexes are developed by dense atomic displacements, which are taken into account by the displacement-spike model. The re-arrangement of flaws/defects into promising configurations may contribute to the enhancement in electronic and mechanical properties of irradiated materials.[23] These mechanisms are well supported by kinetic Monte–Carlo (KMC) theory. Clustering and recombination are preferred over isolated chain scission at high defect densities. This leads to the generation of stable structures and their modifications.[22]

A lot of research is performed for the enhancement of surface characteristics of polymer (CR-39) via gaseous and metallic implantation of ions. To the best of our knowledge, little to no work has been conducted on surface modification, structural variation, improvement in electrical and optical properties of CR-39 targets via Si ions taken from laser generated Si plasma. In this work the variation in electrical conductivity is correlated with alteration in structural and optical characteristics of implanted CR-39 targets, making them useful in photonic and medical devices, packaging industry, and electronic devices.[9]

An excimer laser system with 120-mJ energy, 248-nm wavelength, 2.5×10^8 W $\cdot$ cm^{-2} laser intensity, and pulse duration of 20 ns has been used for the generation of plasma, as a Si ion source. The Thomson parabola technique using CR-39 detectors was utilized to estimate the ion energy (610 keV) in the fluence range from 5×10^{13} ions $\cdot$ cm^{-2} to 35×10^{16} ions $\cdot$ cm^{-2}. A digital optical microscope and a confocal microscope were utilized to investigate the surface morphology of the Si-ion-implanted CR-39. Raman and UV–Vis spectroscopic techniques were employed to investigate the modifications in structural and optical properties, respectively. The electrical conductivity of the implanted CR-39 was measured by using the four-probe technique. The SRIM simulation[24] is utilized to estimate the total linear energy transfer (LET) and range of 610-keV Si ions that are 63 eV/A and 1.11 μm, respectively.

The novelty of this work is the development of a relation between the enhancement of electrical and optical characteristics of Si-ion-implanted CR-39 and surface structuring. The enhancement in the surface properties (electrical, structural, and optical) makes CR-39 advantageous in industry (medical & packaging), as well as in photonic and electronic devices, such as optical waveguides and optical filters.[9,10]

2. Experimental details

The experimental setup used to detect laser-generated Si plasma ions and measure their flux and energy using CR-39, is presented in Fig. 1.

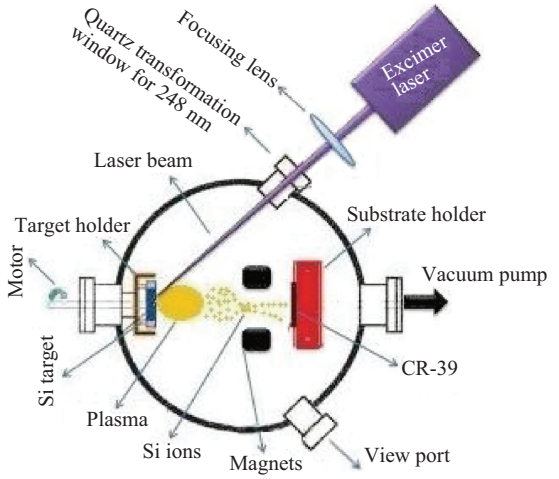


Fig. 1. Schematic diagram of the experimental setup.

An excimer laser (120 mJ, 248 nm, 20 ns, 2.5×10^8 W/cm^2) (EX GAM USA 200) was utilized as a source of irradiation to produce Si plasma. Si targets, circular in shape, with a diameter of 30 mm and a thickness of 5 mm were mounted on a self-designed and fabricated aluminum (Al) holder. A direct current (DC) motor was utilized to rotate the target at a constant speed during implantation to avoid non-uniform ablation and heating of the target. The Thomson parabola scattering technique was used to give a particular path to the Si ions by using two permanent magnets that provided a field strength of 90 mT. The magnetic poles were placed in a Teflon holder at a separation of 50 mm, transverse to the laser-produced Si plasma plume. Four substrates of CR-39 (20 mm $\times$ 10 mm $\times$ 1 mm), (Pershore Moulding, England) were fixed on the substrate holder placed at a distance of 25 mm from the target surface (Si), at an optimum angle of 5° to the normal of the target. The laser irradiation was performed at a pressure of 10^{-9} Torr (1 Torr $= 1.33322 \times 10^2$ Pa). To focus the laser beam on the target surface (Si), a convex lens with a focal length of 50 cm was used. The lens was placed outside the chamber to focus the laser beam at an angle of 45° to the target surface. To check the effect of ion dose on CR-39 substrates, several laser shots were used to expose the Si target. Si plasma was produced forward after interaction of the target with the laser. Coulomb interaction between electrons and ions at the boundary of a laser-induced plasma plume created a space-charge field (according to the space charge acceleration model). This field tended to accelerate Si ions based on their charge-to-mass ratio.[25] After passing through the magnetic field of 90 mT, the energetic Si ions were deflected from their path, based on their charge-to-mass ratio, and struck the substrate surface, resulting in breaking of the chemical bonds within CR-39 and leaving invisible ion tracks. To make the ion-induced tracks visible, irradiated detectors were etched in NaOH solution for 8 hours at 75 °C. The purity and concentration of aqueous NaOH solution throughout the etching process were controlled and the solution was refreshed after each 4 h of etching. After the process of etching, the detectors were taken out of the etching bath, rinsed with distilled water, and then dried in air.

A computer-controlled Motic DM series optical microscope was utilized to study the surface of these dry-etched detectors. Figure 2 illustrates the Thomson Parabola Technique (TPT), demonstrating its use in detecting laser-generated Si plasma ions and measuring their energy and fluence. There were two ion beams: one was the non-deflected central beam that consisted of neutral particles, and the other one was a singly charged Si ion beam deflected by a transverse magnetic field. The deflection value of the beam depends upon the mass, charge, and energy of Si ions.

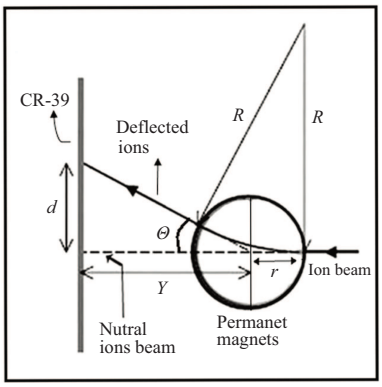


Fig. 2. Thomson parabola technique (TPT): the graphical representation for the measurement, detection of energy, and also for measurement of fluence of laser-generated Si plasma ions.

For the measurement of ion energy, the following equation was utilized[26]

$$E = \frac{e^2 B^2 R^2}{2M} J, \tag{1}$$

where e is the electron charge, B is the magnetic field (90 mT), R is the radius of curvature of ions in the magnetic field, and M is the Si ion mass.

To estimate the radius of curvature of ions in the presence of magnetic field, the following formula is used[26]

$$R = \boldsymbol{r} \cdot \boldsymbol{x} + \boldsymbol{r} \cdot \sqrt{\boldsymbol{x}^2 + 1}. \tag{2}$$

In this equation r (10 mm) is the magnetic field's radius and x is calculated by the relation[26]

$$x = \frac{S}{d}, \tag{3}$$

where s (detector's distance from magnet's center) $= 2.5$ cm, r (radius of magnet) $= 1$ cm, and d is the estimated distance of ion track (estimated by computerized digital microscope), *i.e.*, $d = 55$ μm.

The following formula is used to measure the fluence of laser-generated Si ions[26]

$$\text{Ion fluence} = \frac{\text{number of ions}}{\text{area}}. \tag{4}$$

An area of 5×10^4 μm^2 was selected to count the number of ion tracks on the etched polymer, after exposure to an increasing number of laser pulses. This specific area was measured with a computerized optical microscope. The surface morphology of Si ions-implanted CR-39 was studied by using a confocal microscope. The modifications in structural properties were studied with Raman spectroscopy and variations in optical behavior were studied by using UV-Vis spectroscopy. Electrical conductivity of the implanted polymer was studied by using a self-designed and fabricated four-probe system, which consists of four metallic tungsten tips. For the measurement of the voltage, a voltmeter was attached to the two inner probes. To calculate the resistivity, the following equation was used

$$\rho = \frac{\pi}{\ln 2} d \frac{V}{I} = 4523 d \left(\frac{V}{I}\right), \tag{5}$$

where I is the current provided to the outer probes, V is the voltage across inner probe tips, d is the thickness of CR-39, and ρ is the resistivity. This equation (5) is only applicable for $d \ll S/2$, where S represents the space between probes. The value of d of CR-39 is 1 mm and S is equal to 2.8 mm.

3. Results and discussion

3.1. Surface morphology

Optical microscopy was employed to study variations in surface morphology of Si ion-implanted CR-39 at different fluences of ions. Figure 3 presents micrographic scans of (a) unimplanted polymer and Si ion-implanted polymer at various ion fluences, (b) 5×10^{13}, (c) 15×10^{14}, (d) 20×10^{15}, and (e) 35×10^{16} ions/cm^2, corresponding to 3000, 6000, 9000, and 12000 laser pulses, respectively. Figure 3(a) shows a nearly defect-free surface. After implantation of Si ions, the initial grain structures on the surface of CR-39 are perceived in Figs. 3(b)–3(e). Irregularly shaped, large-sized grains are observed (Fig. 3(b)) at the minimum ion fluence (5×10^{13} ions/cm^2). Cracks and micro-cavities are also seen along the grain boundaries. A decrease in grain size accompanied by diffuse grain boundaries, along with a reduction in both the number and size of cavities, was observed with increased ion fluence up to 20×10^{15} ions/cm^2 (Fig. 3(c)). For an ion fluence of 35×10^{16} ions/cm^2, grains of small size accompanied by distinct and wider grain boundaries are observed. These ion-induced grains are circular in shape, well-organized, and well-defined.

During implantation of Si ions into CR-39, the ion loses energy by three different mechanisms: (i) during inelastic collisions involving bound and free electrons, (ii) elastic collisions between host atoms and implanted Si ions, and (iii) during the exchange of charge between ions and host atoms. During this ion–material interaction, elastic and inelastic collisions result in the transfer of energy and momentum to the matrix and sub-matrix of the polymer, which initiates electronic excitation and ionization in the matrices and sub-matrices of the implanted polymer. The excited electrons thermalize by losing their energy during elastic (less than 100 eV) and inelastic (more than 100 eV) collisions with the host atoms and surface electrons. Consequently, recoil atoms are formed and activated by these mechanisms, and the host atoms lose their energy by electronic and nuclear phenomena until all the electrons and atoms of the host material thermalize by dissipating their energy through electron–phonon coupling.[27]

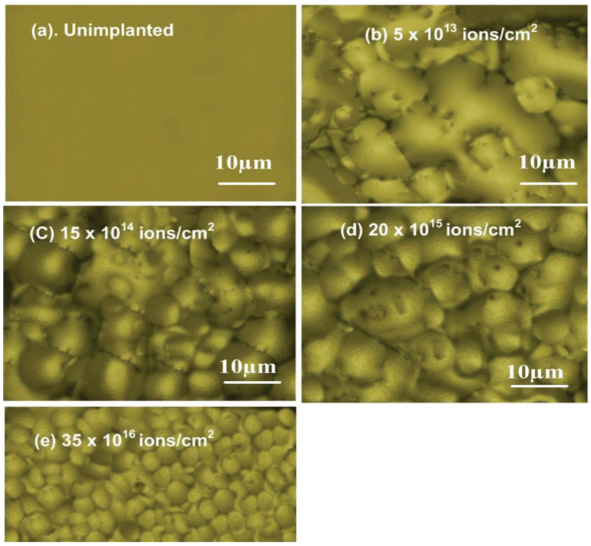


Fig. 3. Surface morphology of (a) pristine and Si ions-implanted targets (CR 39) for 610 keV for various ion fluence values of (b) 5×10^{13} ions$\cdot$cm^{-2}, (c) 15×10^{14} ions$\cdot$cm^{-2}, (d) 20×10^{15} ions$\cdot$cm^{-2}, and (e) 35×10^{16} ions$\cdot$cm^{-2} as a result of increase in number of laser shots from 3000, 6000, 9000 to 12000, respectively.

During the process of ion-material interaction, both phenomena (inelastic and elastic collisions) start simultaneously, which leads to the creation of molecular ions and liberation of secondary electrons. After the ion–polymer interaction, cumulative deposition of an adequate amount of heat per ion results in enhanced local temperature and pressure in the volumetric area, which results in cross-linking, chain scission, bond-breaking, the formation of defects (Frenkel pairs), and liberation of volatile molecules in the lattice/sub-lattice systems of CR-39.[28] The thermal spike model can be utilized to explain the creation of granular morphology. At the start of the Si ion-implantation process, preliminary Si ions result in the formation of an Si-polymer composite along with significantly distorted lattices and sub-lattice systems. These distorted lattice and sub-lattice host atoms receive more energy from the incoming Si ions during the collision phase of the displacement

spike. This results in the rise of surface temperature of the implanted polymer up to thousands of kelvins. The thermal spike region is the high-temperature region. The temperature of the ion-induced thermal spike and the electron–phonon coupling factor are responsible for the energy transfer from excited surface electrons to the host lattice. In the radial direction, at a distance of 7 nm–8 nm, the area of the ion track diminishes progressively and the temperature induced by the ions reduces to 370 K from the track axis.

The implanted ion energy, ion fluence as well as conductivity of the host material influence the area of ion track. Therefore, the thermal spike process leads to a rapid local temperature increase that exceeds the melting point of the polymer. Implantation of Si ions increases the average temperature of the target up to 10^4 K in a short time of 10^{-15} s.[32] This temperature induced by the ions is significantly higher than the melting point of Si (1683 K) and CR-39 (390 K).[27] The following formulae can be utilized to calculate the rise in temperature of the surface after implantation[32,33]

$$T = \frac{1}{\pi \times C_v \times \rho \times r^2} \times \frac{\mathrm{d}E}{\mathrm{d}X}, \tag{6}$$

where ρ is the density of polymer, C_v is the heat capacity of the polymer, T is the increase in surface temperature, $\mathrm{d}E/\mathrm{d}X$ is the linear energy transfer (LET), r is the ion track radius,

$$T = \frac{1}{\pi \times C_v \times r^2} \times \gamma S, \tag{7}$$

where D is the atomic density, S is the ion energy loss per unit length, r is the ion track radius (6 Å–10 Å). The surface temperature after implantation was found in the range of 2.2×10^4 K to 6.2×10^4 K by using the above equations. The calculated surface temperature is much higher than the melting temperature of the polymer (CR-39) and Si. Therefore, due to surface tension, a highly disordered and mismatched solid solution zone was produced by ion implantation with much greater pressure and temperature compared with the region outside this region. This pressure difference provides a driving force to minimize the intrinsic stored surface energy and strain due to which numerous thermally activated host atoms jump along the track to reduce the curvature of the grain boundary.[34] The increase in energy deposition in the absorbing matrices and sub-matrices of the implanted polymeric surface with the increase in the fluence of ions is attributable to the growth of accumulative and collective effects of ions.[35] Therefore, the highest temperature of the spike occurs in the smallest polymeric domains. Only a small amount of heat dissipation occurs due to thermal conduction and the lowest crystallinity of the polymer, which results in an increase in spike life. A further increase in the fluence of ions results in a decrease in the size of grains due to a significant enhancement in the cooling rate.[27] After ion implantation, the high-energy Si ions breach the surface and collide with the atoms of the substrate. Due to these collisions some of the atoms from the CR-39 substrate obtain energy sufficient for displacement, and when this energy exceeds the displacement energy of the lattice of CR-39, the displaced atoms then break free and further collide with the adjacent atoms until the energy gets dissipated. This phenomenon causes the generation of defects on the Si-implanted CR-39 surface. Here the point defect aggregation and migration cause the generation of vacancy clusters leading to the formation of dislocations. Actually, ion implantation induces internal stresses, promotes dislocation movements, and in turn causes enhancement in dislocation density accompanied by cross slip of dislocations and generation of dislocation lines in explicit grain regions. This complex dislocation network causes the generation of complex microstructures like dislocation walls and dislocation tangles. Here, the dislocation tangles are unevenly arranged in the form of dislocation groups that form plastic deformation via recurrent dislocation interactions, while dislocation walls act as the boundaries that divide materials into the subgrains. For increased ion fluence, when the dislocation density approaches a critical value, the rearrangement and annihilation of dislocations cause the formation of low-angle grain boundaries. This phenomenon effectively subdivides the coarse grains into fine grains and in turn causes grain refinement.[29–31]

3.2. Three-dimensional topography

Figure 4 reveals the three-dimensional (3D) surface topography of Si-implanted polymer (60 μm×60 μm) scan area) for various ion fluences: (a) 5×10^{13}, (b) 15×10^{14}, (c) 20×10^{15}, and (d) 35×10^{16} ions/cm^2. The figure shows the formation of micro-sized hillocks whose size depends upon the ion fluence. Figure 4(a) reveals the presence of ion-induced hillock like features.

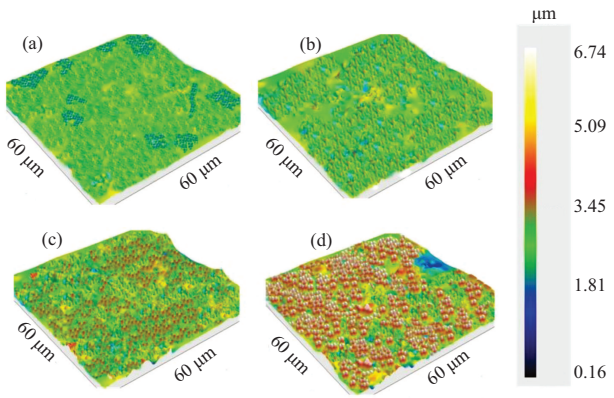


Fig. 4. Three-dimensional surface topography of Si-implanted CR-39 at different ion fluences of (a) 5×10^{13} ions/cm^2, (b) 15×10^{14} ions/cm^2, (c) 20×10^{15} ions/cm^2, and (d) 35×10^{16} ions/cm^2, as a result of increase in number of laser shots from 3000, 6000, 9000 to 12000 respectively, with scan area of 60 μm × 60 μm.

Figures 4(b)–4(d) show the increase in ion fluence results in appearance of well-organized and distinct ion-induced hillocks. Increase in diameter, height, and density of hillocks

are also observed by increasing ion fluence. According to He and Bassim,[36] gases diffused and trapped by points defects along the ion-induced track core are responsible for the generation of hillocks on the implanted surface. The development of hillocks can also be related to the gases relieved (such as, H_2, O_2, CH_4, CO, and CO_2) from the target polymer surface due to chain scission process during ion material interaction.

Thermo-elastically induced stresses in CR-39 matrix caused by ion-induced heating (temperature spike) in the surface and subsurface of implanted material can be utilized to explain the formation of hillocks and nano-cavities. These ion-induced stresses give rise to the pressure in the localized heated volume that surpasses the elastic limit of CR-39 and results in rupturing or phase explosion which is a vital reason for the ejection of melted material from molten pool of implanted zone. Such abrupt increase in ion-induced pressure field is reduced by the generation of hillocks over the surface of CR-39.[37,38] The shape and dimensions of the hillocks depend upon the target surface properties, implanted ion energy, and implantation conditions.[39]

The implanted Si ions slow down and finally come to rest after transferring their energy and momentum to lattice atoms, which causes damage and disorder of the lattice of the implanted polymer. Violent collisions between Si ions and host atoms displace the host atoms from their equilibrium lattice positions, allowing the Si ions to occupy interstitial lattice sites. As a result, stable dimers form between the displaced host atoms and the implanted Si ions.

These ion-induced dimers can relocate more atoms from their normal lattice sites. These dimers have the ability to attract other atoms or ions to make trimers which are responsible for generating lattice distortion and lattice deformation. Subsequently, the variations in nucleation and growth rate of clusters take place. These variations make a momentous change in the size of hillocks which are isolated localized agglomerations of atoms that cannot escape from the irradiated polymer and appear as hillock-like structures due to solidification.[40]

3.3. Raman spectroscopy

The Raman spectra of un-implanted and Si ion-implanted polymers measured at various ion fluences: (a) 5×10^{13}, (b) 15×10^{14}, (c) 20×10^{15}, and (d) 35×10^{16} ions/cm^2 are represented in Fig. 5. CR-39 has monomer structure that is validated by the presence of all the identified peaks (1119, 1287, 1451, 1643, 1737, 2913, and 2958 cm^{-1}) in the unimplanted target.[9] The observed peak at wave number of 1119 cm^{-1} presents C–O–C stretching mode and the peak seen at 1287 cm^{-1} is attributable to the stretching mode of C–O. Peaks identified at 1451, 1643, and 1737 cm^{-1} represents bending mode of C–H and stretching modes of C=C and C=O respectively. Strong bands detected at 2958 cm^{-1} and 2913 cm^{-1} shows the presence of asymmetric stretching and symmetric stretching modes of –CH_2– respectively. Significant alterations in the polymer's chemical structure occur due to the complete breakdown of bonds after Si ion implantation, results in complete removal of C–O–C band initially available at 1119 cm^{-1}.[9] Two peaks of C–O and C–H bands are identified at 1451 cm^{-1} and 1287 cm^{-1} respectively. The decrease in intensity of the above-mentioned bands with increase in ion fluence up to 20×10^{15} ions/cm^2 is credited to ion-induced damage to the matrix, which weakened the C–O and C–H bonds. For fluence value of 35×10^{16} ions/cm^2, the peaks of C–O and C–H bands completely vanished because of intrinsic chain scissoring of the polymer by ion implantation.

From Fig. 5, we can also see that the peaks appearing at 1643 cm^{-1} and 1737 cm^{-1} representing C=C and C=O bonds show a drastic reduction in peak intensity after implantation with ions at a fluence of 25×10^{14} ions/cm^2. It is attributable to carbon ester obliteration in the polymer (CR-39) and is consistent with the degradation of the polymer reported by Constantini *et al.*[41] The reduction in the intensity of these peaks was due to the low degree of polymerization. The double bonds are always lost when a monomer undergoes the polymerization process to form a polymer. The complete disappearance of these peaks at maximum fluence is attributable to polymer degradation by chain folding and breaking of carbonyl bonds,[42] which leads to the formation of sp2 carbon cauterization and unsaturated bonds in implanted CR-39. Interestingly, after implantation at maximum fluence (35×10^{16} ions/cm^2), the bands present at 1287, 1119, 1643, 1451, and 1737 cm^{-1} vanished completely owing to significant variations produced in the chemical structure of the polymer.[9] From Fig. 5, at maximum fluence after implantation, a significant decrease in the intensity of –CH_2– at 2913 cm^{-1} and 2958 cm^{-1} was also observed. The decrease in the content of H_2 in the implanted target is the vital reason for this reduction. A similar diminution in the band intensity of the CH_2 group in CR-39 after irradiation with N ions and protons has already been observed by Sharma and Yamauchi respectively.[9,43] After Si ion implantation, a new peak appeared at 890 cm^{-1}, corresponding to Si–C.[44] This suggests that ion implantation ruptures the original bonds of the polymer, leading to free radical cross-linking, chain scission, and related processes. These phenomena were accountable for the growth of new Si–C=O bonds.[9] Ion radiation damage and the incorporation of a specific quantity of Si atoms into the polymer matrix were the primary factors driving the formation of the new phase. The enhancement in peak intensity of Si–C with increasing ion fluence was attributed to the nucleation of Si–C-rich clusters and the carbonization of the track volume.[45] An amorphous layer of carbon was generated on the surface and subsurface of the CR-39 material as a result of

Si ion implantation. This amorphous carbon layer's electronic structure consists of a network of sp^2 and sp^3 bonding sites. To achieve a state of minimum energy, these structures self-organize accordingly.[46] The breaking of long chains, bond scission, lattice distortions, complete disappearance of various peaks, Frankel defects, and new phase formation were the phenomena that took place due to Si ion implantation in response to energy deposition and momentum transfer to the host lattice and sublattice in the vicinity of the ion tracks. Because of this, extensive stresses, pressure spikes, and temperature spikes were generated in the cascade volume of the target material that appears in the form of grains (Fig. 3) and hillocks (Fig. 4).

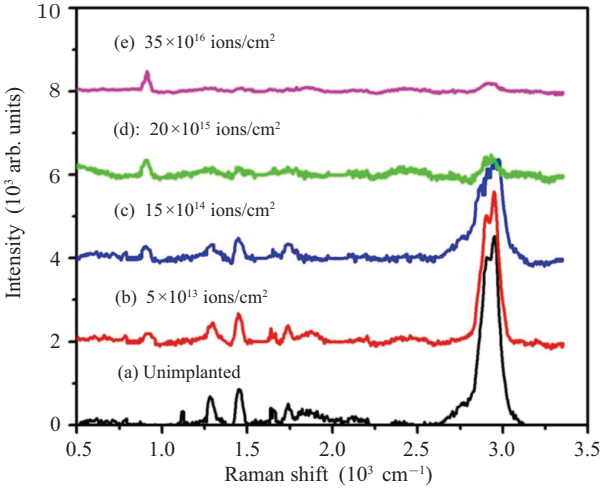


Fig. 5. The Raman spectrographs of un-implanted and implanted CR-39 targets, for various Si ion fluences ranging from 5×10^{13} ions/cm^2 to 35×10^{16} ions/cm^2, as a result of increase in number of laser shots from 3000, 6000, 9000 to 12000, respectively.

3.4. UV–Vis spectral analysis

The UV-vis spectroscopy was used to analyze changes in optical properties following ion implantation. Figure 6 presents the UV-vis spectra of unimplanted CR-39 polymer and CR-39 targets implanted with Si ions at various ion fluences: (a) 5×10^{13}, (b) 15×10^{14}, (c) 20×10^{15}, and (d) 35×10^{16} ions/cm^2, corresponding to laser shots of 3000, 6000, 9000, and 12000, respectively, at an intensity of 2.5×10^8 W/cm^2. Prior to ion implantation, the CR-39 target exhibits approximately 96% transmittance in the visible region, ranging from 350 nm to 550 nm. The polymer electrons cannot completely absorb the incident light because all the host electrons are tightly bound to their atoms.[13] Transmittance behavior of the implanted CR-39 depends upon many parameters like incident angle, ion fluence, energy, and chemical composition of the target material. An increase in fluence of ions leads to a reduction in optical transmittance. At a fluence of 5×10^{13} ions/cm^2, the Si ion-implanted polymer exhibits a transmittance of 90%. This transmittance decreases with increasing fluence, reaching 75% at a fluence of 35×10^{16} ions/cm^2. Optical (Fig. 3) and Raman spectroscopy (Fig. 5) results support the results of UV-vis spectroscopy. The emission of carbon atoms from the polymer's main chain is responsible for changes in optical transmission properties during ion implantation which lead to the creation of graphite-like precipitates/clusters.[47] The degree of graphitization and formation of sp^2 carbon clusters in the implanted CR-39 are attributable to the observed changes in optical transmission values. The granular morphology and hillock-like features depicted in Figs. 3 and 4 contribute to light scattering, leading to a reduction in the optical transmittance of the polymer.[48]

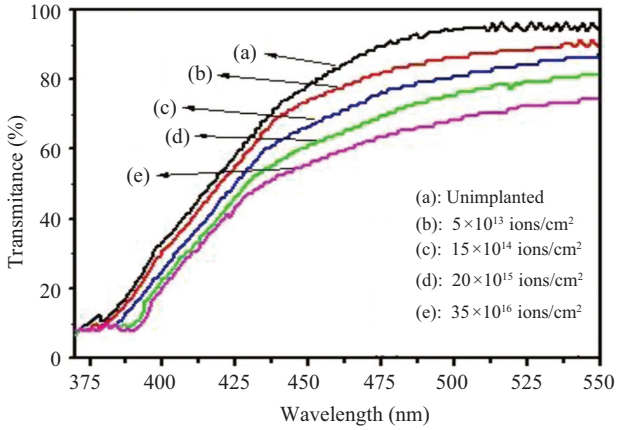


Fig. 6. UV-visible transmission spectra of un-implanted and Si ion implanted CR-39 targets irradiated with four different ion fluences of (b) 5×10^{13} ions/cm^2, (c) 15×10^{14} ions/cm^2, (d) 20×10^{15} ions/cm^2, and (e) 35×10^{16} ions/cm^2 for different laser shots ranging from 3000 to 12000.

Significant intermixing of incident Si ions with carbon content in polymer matrices and sub-matrices causes the breakup of the C–H bond due to disordering effects produced on the polymer surface and results in the development of conjugated and unsaturated bonds.[49] The surface electrons absorb the energy of incident Si ions that serves as a localized heat source, causing the temperature of the implanted surface to rise significantly, reaching thousands of degrees Celsius. The host atoms of the polymer absorb energy of incident Si ions in both the visible and ultraviolet spectrum involving transitions of n, σ, and π orbitals from their ground state to higher energy states. The temperature induced by ions significantly affects the degree of the conjugated structure and is attributable to the formation of n-electrons (π-electrons). The degree of conjugation is responsible for changing the optical and electrical properties in Si ion-implanted CR-39.[9] A significant decrease in the transmittance rate is highly sensitive to ion fluence, absorbed dose, and the nature and energy of the ions.[50]

3.5. Electrical conductivity

Figure 7 shows the behavior of electrical conductivity of CR-39 after implantation with 610-keV Si ions for var-

ious fluences: (a) 5×10^{13}, (b) 15×10^{14}, (c) 20×10^{15}, and (d) 35×10^{16} ions/cm^2 corresponding to laser shots of 3000, 6000, 9000, and 12000, respectively, at an intensity of 2.5×10^8 W/cm^2. The reported electrical conductivity value for unimplanted CR-39 is 10^{-9} S/cm^1. This low conductivity is attributed to the absence of the system of charge transport in the matrices and sub-matrices. Si ion implantation at a fluence value of 5×10^{13} ions/cm^2 results in a significant increase in electrical conductivity from 10^{-9} S/cm^1 to 10^{-7} S/cm^1. Further, the increase in ion fluence from 15×10^{14} ions/cm^2 to 35×10^{16} ions/cm^2 results in an additional enhancement of the electrical conductivity of the implanted polymer. This increase in conductivity is attributable to the growth of conjugated carbon–oxygen, carbon–carbon, carbon–hydrogen, and silicon–carbon bonds and formation of cross-linked morphology which provide conducting bridges and paths for mobility of charge carriers.[27,32] The remarkable enhancement in electrical conductivity after implantation is attributable to alterations in the chemical, structural, and transmission properties. The formation of Si-like precipitates/clusters by ion implantation due to electronic energy transfer can cause an increase in conductivity of the implanted polymer.[9] These clusters are also formed due to breaking of intrinsic bonds in the grain structure of polymeric long chains due to the large energy transfer by the incident Si ions per ion track that generates conducting bridges among polymeric grains owing to the intermixing of implanted Si ions and host atoms. Cross linking, formation of π-electrons, and free radicals in ion-produced dense carbon, allow the hopping of electrons amongst the polymeric grains and increase its conductivity.[51] The sizes of carbonaceous and ion-induced Si clusters increase with an increase in carbon and Si atoms per cluster which results in a momentous increase in electrical conductivity of the implanted CR-39.[45] The increase in electrical conductivity in the implanted polymer can also be attributed to the enhanced density and mobility of charge carriers.[52] The formation of carbonaceous clusters also depends upon the deposition of energy on the polymer surface.[45] The ion-induced precipitates/clusters are comprised of sp^2 island structure and conjugated carbon–carbon, carbon–oxygen, carbon–hydrogen, and silicon–carbon bonds which result in a decrease in the gap energy between conduction and valence bands. As a small amount of energy is required by π-electrons for the transition, therefore the loosely bound π-electrons of valence bands can be excited easily to the conduction bands by using the kinetic energy from the implanted 610-keV Si ions. As a result, the electrical conductivity in the modified layer of the implanted polymer increases by increasing ion fluence.[9] Raman spectral analysis (Fig. 5) confirms the formation of carbon–carbon, carbon–oxygen, carbon–hydrogen, and silicon–carbon bonds in the implanted polymer. The significant improvement in electrical conductivity by Si implantation is strongly correlated with surface morphology.[53,54]

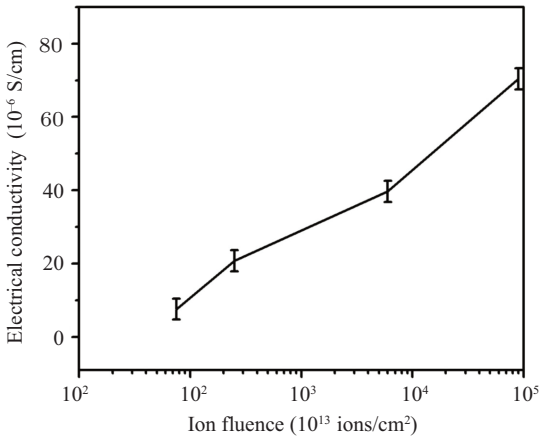


Fig. 7. The study of the electrical conductivity values of CR-39 after implantation for various Si ion fluences ranging from 5×10^{13} ions/cm^2 to 35×10^{16} ions/cm^2, as a result of increase in number of laser shots from 3000, 6000, 9000 to 12000, respectively.

The primary method for enhancing electrical conduction is to reduce the scattering of π-electrons and the implanted Si ions within the chain-folded CR-39 crystallites, lattices, and sub-lattices.[55]

3.6. SRIM speculated damage profiles

Impact of energetic ions on a polymer surface results in the exchange of their energy with surface electrons and lattice atoms, which dislodge them from their locations. This energy loss takes place mainly through inelastic and elastic collisions. The penetration of ions into the polymer target is highly dependent on the species of the ions and the atomic structure and chemical properties of the substrate. Moreover, the lack of preservation of ion energy, as a result of the collisional interaction of the ions with lattice atoms governed by the theory of electronic stopping power (S_e) and nuclear stopping power (S_n), results in the displacement of the atoms that form the lattice structure. This disturbance causes point defects in the material, such as interstitials and vacancies, induced on the target by ions.[56] For ions with high energies, nuclear stopping power (S_n) has a tendency to lead the energy loss process. In contrast, for heavier and more energetic ions, electronic stopping power (S_e)) becomes the prevailing mechanism. To investigate the complex damage profile resulting from the irradiation of CR-39 with 610-keV Si ions, simulations were conducted using SRIM-2013 software.[57]

Figures 8(a) and 8(b) represent the 2D longitudinal view and the distribution of ions at 610-keV Si ions irradiation of CR-39 target. Through the simulation results, the mean estimated range of Si ions is ~ 1.1 μm, but the rest of the parame-

ters, such as longitudinal straggling, lateral straggling, S_e, and S_n have approximate values of 1193 Å, 1277 Å, 4.6 keV/μm and 6.3 keV/μm. The implanted Si ions produce the electronic excitation and point defects such as interstitials and vacancies along their trajectory, potentially resulting in both longitudinal and lateral damage within the lattice of target material.[58]

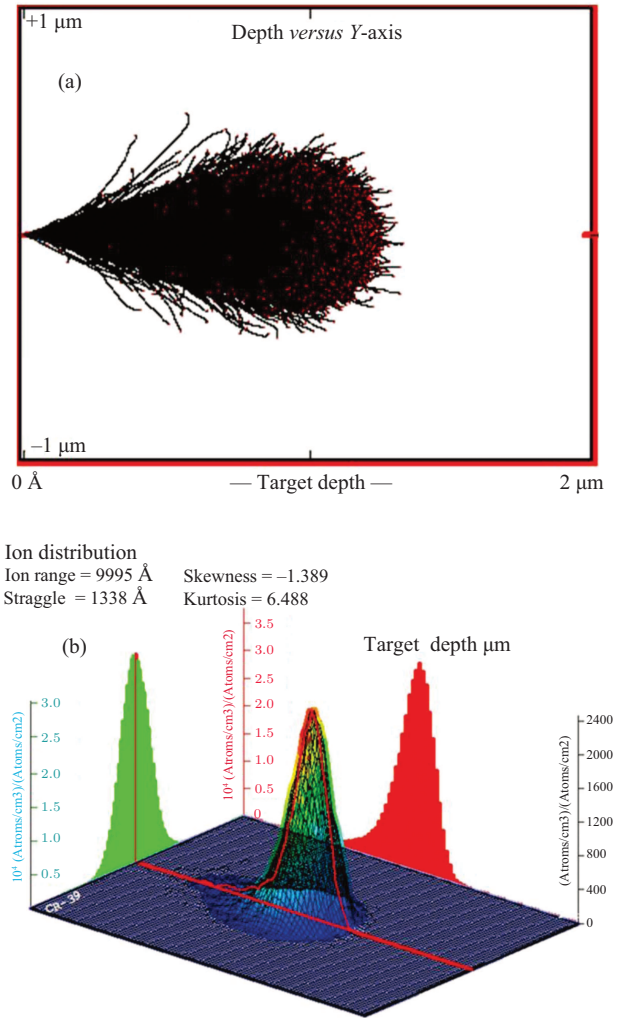


Fig. 8. (a) The 2D longitudinal view of Si ions at 610 keV, irradiation of CR-39 target using SRIM speculated damage profiles. (b) The longitudinal distribution of Si ions, at 610 keV, irradiation of CR-39 target using SRIM speculated damage profiles.

4. Conclusions

The effect of laser generated plasma Si ions implantation over the morphological features, optical characteristics, structural properties, and electrical behavior induced by 610-keV Si ions in the CR-39 matrix has been investigated in the current research. To achieve this, Si ions are implanted into the surface of CR-39 for fluences ranging from 5×10^{13} ions/cm^2 to 35×10^{16} ions/cm^2 in conjunction with an increasing number of laser pulses from 3000 to 12000. Optical microscope shows the presence of irregular-shaped grains along with cracks and cavities across the grain boundaries for the lowest ion fluence (5×10^{13} ions/cm^2). Small, circular-shaped grains with distinct and broader grain boundaries are clearly visible at maximum fluence (35×10^{16} ions/cm^2). For the increased ion fluence, the dislocation density approaches a critical value of the re-arrangement in annihilation of dislocations, causing the formation of low-angle grain boundaries. This phenomenon effectively subdivides the coarse grains into fine grains and in turn causes grain refinement. Confocal microscope investigations reveal the growth of hillocks whose density, height, and diameter increase with the increase in ion fluence. Point defects generated by the diffused and trapped gases along the ion-induced track core are responsible for the generation of hillocks on the implanted surface. Thermo-elastically induced stresses in the CR-39 matrix, caused by surface and subsurface heating of the implanted material, also result in hillock formation. Raman spectroscopy shows the creation of a novel band of Si–C with increasing intensity with the increase in ion fluence owing to the carbonization of the track volume and nucleation of Si–C-rich clusters after ion implantation. The formation of grains, cavities, and hillocks, along with ion-induced structural alterations is responsible for a decrease in the optical transmittance of the implanted polymer. The development of carbonaceous structures and the formation of a conductive layer result in an increase in the conductivity of the implanted polymer with an increase in the fluence of ions. The increased electrical conductivity of CR-39 is well correlated with its structural variations, optical transmission behavior, and surface morphology. The improved morphological features, structural properties, optical characteristics, and electrical behavior of CR-39 make it beneficial for applications in packaging and electronic industries, medical sciences, and photonic devices.

References

[1] Rai V N, Singh J P, Yueh F Y and Cook R L 2003 *Laser Part. Beams* **21** 65
[2] Harilal S S, Tillack M S, O'Shay B, Bindhu C V and Najmabadi F 2004 *Phys. Rev. E* **69** 026413
[3] Torrisi L, Margarone D, Gammino S and Andó L 2008 *Radiat. Eff. Defects Solids* **163** 261
[4] Dirnberger L, Dyer P E, Farrar S R and Key P H 1993 *AIP Conf. Proc.* **288** 349
[5] Khwairakpam O S, *et al.* 2024 *Nucl. Instrum. Methods Phys. Res. B* **548** 165249
[6] Wen Z, Xu Z, Wang C, Zhang Q, Si M, Song X, Dou Y, Li B and Lin J 2024 *Vacuum* **224** 113145
[7] Khan M R, Haq S U, Abbas Q and Nadeem A 2023 *Spectrochim. Acta B* **200** 106612
[8] Springham S V, Lee S and Rafique M S 2000 *Plasma Phys. Control. Fusion* **42** 1023
[9] Sharma T, Aggarwal S, Sharma A and Kumar S 2007 *J. Appl. Phys.* **102** 063527
[10] Othman S M, El-Mansy I A, El-Badawy A S and Ghanim E H 2024 *Appl. Radiat. Isot.* **208** 111253
[11] Sadeq M S, Hassan N M, El-Saftawy A A and Sedqy E M 2024 *Radiat. Phys. Chem.* **218** 111537
[12] Pauleau Y 1989 *Materials and Processes for Surface and Interface Engineering* (London: Springer)

[13] Teixeira F S, Salvadori M C, Cattani M and Brown I G 2009 *J. Appl. Phys.* **105** 064313

[14] Bouffard S, Balanzat E, Leroy C, Busnel J P and Guevelou G 1997 *Nucl. Instrum. Methods Phys. Res. B* **131** 79

[15] Zhang S, Liu Y, Lv S and Cheng J 2023 *Nucl. Instrum. Methods Phys. Res. B* **543** 165097

[16] Sadeq M S, Hassan N M, El-Saftawy A A and Sedqy E M 2024 *Radiat. Phys. Chem.* **218** 111537

[17] Badry B A E, Zaki M F, Abdul-Kader A M, Hegazy T M and Morsy A A 2009 *Vacuum* **83** 1138

[18] Resta V, *et al.* 2013 *Nucl. Instrum. Methods Phys. Res. B* **312** 42

[19] Bashir S A, Ali S, Kalsoom U I, Rafique M S and Alshehri A M 2024 *Heliyon* **10** e34553

[20] Wante H P Y, *et al.* 2025 *Eur. Phys. J. Plus* **140** 837

[21] Liu Y, Li S S and Cheng J P 2024 *Nucl. Instrum. Methods Phys. Res. B* **556** 165432

[22] Azevedo A M, Monteiro S N and Veiga-Júnior V F 2025 *Polymers* **17** 1110

[23] Szenes G 1995 *Phys. Rev. B* **51** 8026

[24] Ziegler J F 2013 SRIM

[25] Bykovskii Y A, Degtyarenko N N, Kondrashov V E and Lovetskii E E 1974 *Phys. Tech. Phys.* **18** 1597

[26] Rafique M S, Rahman M K, Rehman A, Siraj K and Khan M F 2007 *Laser Phys.* **17** 282

[27] Fink D 2004 *Fundamentals of Ion Irradiated Polymers* (Berlin: Springer)

[28] Nouh S A, Salam M H A and Morsy A A 2003 *Radiat. Meas.* **37** 25

[29] Zeng Y, Tang J, Zhu J, Shen X and Ling Y 2025 *J. Mater. Res. Technol.* **38** 3218

[30] Sun X, Zhang Y, Wang L, Li R and Wang J 2023 *Nucl. Instrum. Methods Phys. Res. B* **541** 123

[31] Kumar T R, Murty R M, Suresh A S and Panigrahi B B 2024 *J. Alloys Compd.* **951** 170018

[32] Wise D L, *et al.* 1998 *Electrical and Optical Polymer Systems* (New York)

[33] Lucchese R R 1987 *J. Chem. Phys.* **86** 443

[34] Mio A M, *et al.* 2011 *J. Non-Cryst. Solids* **357** 2197

[35] Ahmad S, *et al.* 2014 *Nucl. Instrum. Methods Phys. Res. B* **325** 5

[36] Adhikari A R, *et al.* 2014 *J. Surf. Eng. Mater. Adv. Technol.* **4** 326

[37] Wang T S, *et al.* 2009 *Nucl. Instrum. Methods Phys. Res. B* **267** 2605

[38] Koubassov V, *et al.* 2004 *Appl. Phys. A* **79** 499

[39] Sattler K D (ed.) 2010 *Handbook of Nanophysics* (Boca Raton: CRC Press)

[40] Abbaschian R, Abbaschian L and Hill R E R 1994 *Physical Metallurgy Principles*

[41] Costantini J M, *et al.* 2005 *Nucl. Instrum. Methods Phys. Res. B* **234** 458

[42] Mallick B, *et al.* 2008 *Radiat. Eff. Defects Solids* **163** 161

[43] Yamauchi T, *et al.* 2001 *Radiat. Meas.* **34** 69

[44] Socrates G 2004 *Infrared and Raman Characteristic Group Frequencies*

[45] Fink D, *et al.* 1996 *Nucl. Instrum. Methods Phys. Res. B* **111** 303

[46] Kondyurin A and Bilek M 2008 *Ion Beam Treatment of Polymers* (Elsevier)

[47] Davenas J, *et al.* 1988 *Nucl. Instrum. Methods Phys. Res. B* **32** 136

[48] Stepanov A L and Khaibullin R I 2004 *Rev. Adv. Mater. Sci.* **7** 108

[49] Shekhawat N, *et al.* 2011 *J. Appl. Phys.* **109** 083513

[50] Yamauchi T, Taniguchi T and Oda K 1999 *Radiat. Meas.* **31** 261

[51] Forrest S R, *et al.* 1982 *Appl. Phys. Lett.* **41** 708

[52] Nathawat R, *et al.* 2008 *Nucl. Instrum. Methods Phys. Res. B* **266** 4749

[53] Wan C L, *et al.* 2006 *Phys. Rev. B* **74** 144109

[54] Ziaie F, *et al.* 2007 *Radiat. Phys. Chem.* **76** 1684

[55] Shi X and Chen L 2004 *Appl. Phys. Lett.* **84** 2301

[56] Chae S, Kim Y S and Rafique M S 2016 *Optik* **127** 9152

[57] Stoller R E, *et al.* 2013 *Nucl. Instrum. Methods Phys. Res. B* **310** 75

[58] Netta C B, *et al.* 2025 *Radiat. Phys. Chem.* **226** 112275